Mechanisms and absolute quantum yield of upconversion luminescence of fluoride phosphors

A. A. Lyapin[1,*], S. V. Gushchin[1], A. S. Ermakov[1], S. V. Kuznetsov[2], P. A. Ryabochkina[1], V. Yu. Proydakova[2], V. V. Voronov[2], P. P. Fedorov[2], and M. V. Chernov[1]

[1]*National Research Ogarev Mordovia State University, Saransk 430005, Mordovia, Russia*
[2]*Prokhorov General Physics Institute of the Russian Academy of Sciences, Moscow 119991, Russia*
**Corresponding author: andrei_lyapin@mail.ru*

Received May 19, 2018; accepted July 25, 2018; posted online August 31, 2018

Mechanisms of upconversion luminescence (UCL) of SrF_2:Er phosphors corresponding to the $^4G_{11/2} \rightarrow {}^4I_{15/2}$, $^2H_{9/2} \rightarrow {}^4I_{15/2}$, $^4F_{5/2} \rightarrow {}^4I_{15/2}$, $^4F_{7/2} \rightarrow {}^4I_{15/2}$, $^2H_{11/2} \rightarrow {}^4I_{15/2}$, $^4S_{3/2} \rightarrow {}^4I_{15/2}$, $^4F_{9/2} \rightarrow {}^4I_{15/2}$, and $^4I_{9/2} \rightarrow {}^4I_{15/2}$ transitions upon excitation of the $^4I_{11/2}$ level of Er^{3+} ions were investigated. Energy transfer upconversion processes are responsible for the populating of the $^2H_{9/2}$, $^2H_{11/2}$, $^4S_{3/2}$, and $^4F_{9/2}$ levels. Cooperative process is the dominant mechanism of luminescence from $^4S_{3/2}$ and $^4F_{9/2}$ levels for SrF_2:Er with high concentrations of Er^{3+} ions. The UCL from $^4G_{11/2}$ and $^4F_{5/2}$ is explained by excited-state absorption. Cross-relaxation processes take part in the population of $^4F_{9/2}$ and $^4I_{9/2}$ levels. For quantifying material performance, the Er^{3+}-concentration dependence of UCL and the absolute quantum yields of SrF_2:Er were studied. The most intensive visible luminescence was obtained for SrF_2:Er (14.2%) with 0.28% maximum quantum yield.

OCIS codes: 190.7220, 160.2540, 140.5680.
doi: 10.3788/COL201816.091901.

Upconversion luminescence (UCL) materials have been extensively investigated since the mid-1960s and have found different applications in photonics: solar cell, sensors, detection, solid-state lasers, visualizers, etc. In the last decade, the field of rare-earth (RE) doped upconversion (UC) nanoparticles, powders, and phosphors is rapidly progressing from the fundamental understanding of photoluminescence properties to a lot of applications in medicine and biology[1–3].

UC properties of RE ions strongly depend on the host. Highly efficient UCL is observed for fluorite-type materials MF_2:RE (M = Ca, Sr, Ba)[4–9] because they have low phonon energy (~366 cm^{-1} of SrF_2) [10] and the tendency to form multiple cluster configurations even when the doping concentration is low[11–14]. Low phonon energy allows the lifetime of the intermediate levels to be increased. The clustering effect reduces the distance between Er^{3+} ions and thereby increases the probability of an energy transfer process between them, which is beneficial for achieving efficient UCL.

Er^{3+}-doped phosphors are demonstrated efficient UCL upon excitation of different infrared energy levels of Er^{3+} ions. At present, a large number of papers are devoted to the study of UCL of Er^{3+}-doped fluoride and oxide phosphors upon excitation by laser radiation at about 980 nm[15–22]. UCL of SrF_2:Er powders prepared by combustion synthesis ions was demonstrated upon excitation of the $^4I_{11/2}$ level of Er^{3+} ions by Rakov[15]. However, we have not found publications of the mechanisms and absolute quantum yield Φ_{UC} of UCL of SrF_2:Er phosphors.

To develop new UC phosphors for the different applications fields, the nature of UC and luminescence efficiency need to be investigated. Thus, our research is focused on a detailed study of the mechanisms of UCL of SrF_2:Er phosphors upon 972 nm laser diode (LD) excitation. Also, the Er^{3+}-concentration dependence of UCL and the absolute photoluminescence quantum yields of SrF_2:Er were studied.

The SrF_2:Er (mole fractions of Er^{3+} ions are 1.6%, 3.4%, 6.0%, 8.8%, 14.2%, 18.3%, and 21.3%) phosphors were synthesized by using a co-precipitation with the aqueous nitrate solution technique[23–25]. The initial reagents for the synthesis of fluoride powders were strontium nitrate (99.99% for metallic impurities), erbium nitrate five hydrate (99.99% for metallic impurities) produced by LANHIT (Moscow, Russia), ammonium fluoride, and double distilled water. An erbium and strontium nitrate aqueous solution of 0.08 M (1 M = 1 mol/L) concentration was added dropwise to a 7% excess of 0.16 M aqueous ammonium fluoride under intense stirring. After precipitation of SrF_2:Er solid solution the matrix solution was decanted. The obtained powders were dried in air at 45°C (5 h) and annealed in platinum crucibles in air at 600°C (1 h).

The luminescence of the Er^{3+} ions excited by an LD at 972 nm was recorded using a Horiba FHR1000 spectrometer. The focused excitation beam diameter on the samples was 712 μm. The incident excitation power was 100 and 250 mW.

The luminescence rise and decay were recorded from $^4G_{11/2}$ (379 nm), $^2H_{9/2}$ (407 nm), $^4F_{5/2}$ (449 nm), $^4F_{7/2}$ (486 nm), $^2H_{11/2}$ (521 nm), $^4S_{3/2}$ (548 nm), $^4F_{9/2}$ (668 nm), and $^4I_{9/2}$ (801 nm) levels of Er^{3+}. For excitation of the $^4I_{11/2}$ level, we used a Ti:sapphire laser

model LX329 (Solar LS) at a wavelength of 972 nm. The duration of the exciting pulse was 20 ns. The excitation pulse repetition frequency was 10 Hz. The rise and decay of luminescence were examined by a Tektronix TDS 2022C digital oscilloscope (200 MHz).

The integrating sphere method was used to measure the absolute photoluminescence quantum yield[26,27]. The system consists of the OL IS-670-LED integrating sphere, an OL-770 UV/VIS (Gooch & Housego) spectroradiometer, and a monochromator-spectrograph M833 (Solar LS). The incident excitation power was measured using a UP19K-110F-H9-D0 (Standa) power meter. All measurements were performed at room temperature.

Upon excitation of the $^4I_{11/2}$ level, the visible and near-infrared UCL spectra of Er^{3+} ions in SrF_2:Er phosphors at 300 K corresponding to $^4G_{11/2} \rightarrow {}^4I_{15/2}$, $^2H_{9/2} \rightarrow {}^4I_{15/2}$, $^4F_{5/2} \rightarrow {}^4I_{15/2}$, $^4F_{7/2} \rightarrow {}^4I_{15/2}$, $^2H_{11/2} \rightarrow {}^4I_{15/2}$, $^4S_{3/2} \rightarrow {}^4I_{15/2}$, $^4F_{9/2} \rightarrow {}^4I_{15/2}$, and $^4I_{9/2} \rightarrow {}^4I_{15/2}$ transitions were recorded (Fig. 1). The most intense luminescence was observed in the green and red spectral ranges. The same UCL spectra were observed for all SrF_2:Er samples. The absorption transition, luminescence transitions, and possible UC mechanisms of Er^{3+} ions in SrF_2:Er phosphors are shown in Fig. 2.

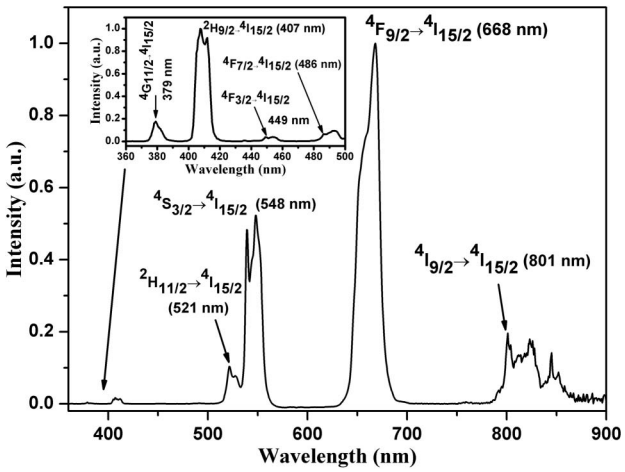

Fig. 1. UCL spectra of SrF_2:Er (14.2 mol.%) in the visible and near-infrared spectral ranges.

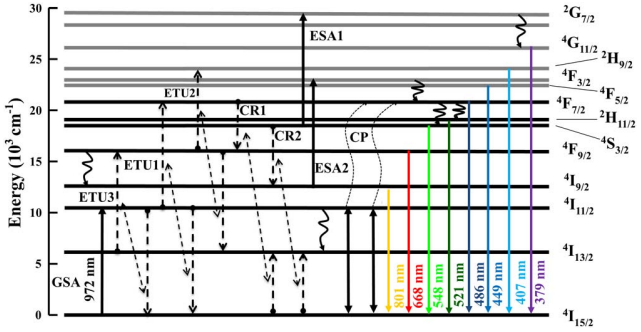

Fig. 2. Absorption transition, luminescence transitions, and UC mechanisms of Er^{3+} ions in SrF_2:Er.

Next, two experimental methods to determine mechanisms of UCL in SrF_2:Er phosphors were applied. First, excited-state dynamics of SrF_2:Er phosphors were investigated. Second, we studied the excitation power density (P) dependence of UCL.

From literature it is known that excited-state absorption (ESA), energy transfer UC (ETU), and cooperative processes (CPs) are dominated mechanisms of UCL in Er^{3+}-doped materials upon excitation of the $^4I_{11/2}$ level[15–19,21,22,28,29]. We recorded the rise and decay luminescence of Er^{3+} ions from $^4G_{11/2}$ (379 nm), $^2H_{9/2}$ (407 nm), $^4F_{5/2}$ (449 nm), $^4F_{7/2}$ (486 nm), $^2H_{11/2}$ (521 nm), $^4S_{3/2}$ (548 nm), and $^4F_{9/2}$ (668 nm) levels upon excitation of the $^4I_{11/2}$ level. The ESA process leads to an immediate rise of luminescence within the experimental time resolution and a subsequent fast decay corresponding to the relaxation time of the energy level. In contrast, luminescence originating from ETU and CP has a rise part after pulsed excitation. Also, ETU and CP persist after pulsed excitation much longer than the lifetime of the energy level. The nature of the ETU and CP processes is ion–ion interaction of RE ions. Both ETU and CP can simultaneously be responsible for the UCL in a material. But commonly CPs are less effective than ETU ones by 4–5 orders of magnitude[30].

Figure 3 presents the rise and decay of the luminescence of Er^{3+} ions from $^2H_{9/2}$ [Fig. 3(a)], $^2H_{11/2}$ [Fig. 3(b)], and $^4S_{3/2}$ [Fig. 3(c)] levels. For all samples, the luminescence from the $^2H_{9/2}$, $^2H_{11/2}$, and $^4S_{3/2}$ levels exhibits a slow rise and slow decay after the excitation pulse (20 ns),

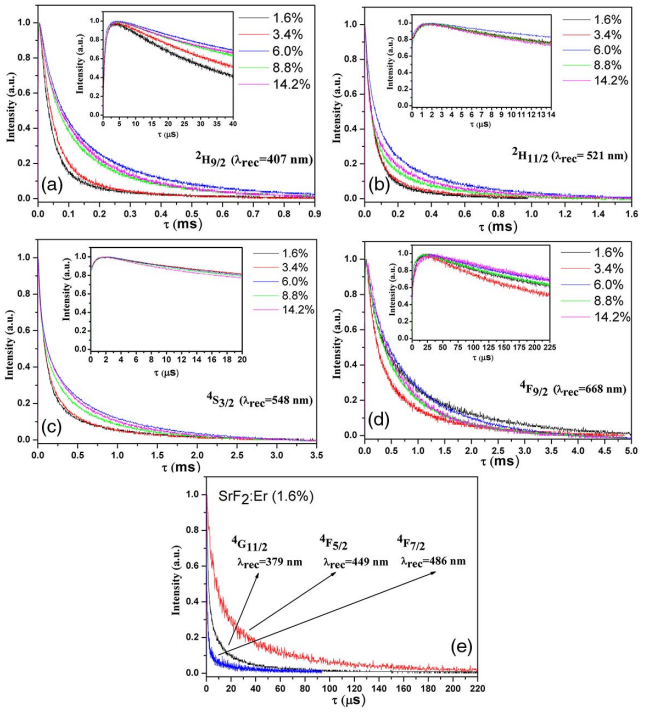

Fig. 3. Luminescence rise and decay from (a) $^2H_{9/2}$, (b) $^2H_{11/2}$, (c) $^4S_{3/2}$, (d) $^4F_{9/2}$, (e) $^4G_{11/2}$, $^4F_{5/2}$, $^4F_{7/2}$ levels of Er^{3+} ions in SrF_2:Er.

indicating that ETU processes contribute to populating these levels. The decay time of the luminescence from the $^2H_{9/2}$, $^2H_{11/2}$, and $^4S_{3/2}$ levels increases with increasing concentration of Er^{3+} ions from 1.6% to 6%. These time dependences are explained by increasing the efficiency of the ETU1 ($^4I_{11/2} + {}^4I_{11/2} \rightarrow {}^4F_{7/2} + {}^4I_{15/2}$) and ETU2 ($^4F_{9/2} + {}^4F_{9/2} \rightarrow {}^2H_{9/2} + {}^4I_{13/2}$) processes. Upon further increasing of the concentration of Er^{3+} ions, the decay time begins to decrease. Su *et al.*[28] showed that the lifetime of the intermediate $^4I_{11/2}$ and $^4I_{13/2}$ levels of the Er^{3+} ions in the SrF_2:Er crystals begins to decrease with increasing concentration of Er^{3+} ions (approximately from 4 mol.%). This explains the reduced decay time of blue and green luminescence for heavily-doped SrF_2:Er phosphors.

The rise and decay of luminescence from the $^4F_{9/2}$ level were detected [Fig. 3(d)]. The luminescence from the $^4F_{9/2}$ level exhibits a slow rise and slow decay after the excitation pulse. This phenomenon is direct evidence of populating of the $^4F_{9/2}$ level by the ETU process. The dependence of the decay of UCL from the $^4F_{9/2}$ level on the concentration of Er^{3+} ions is complex. In our opinion, this is caused by a competition of radiative relaxation ($^4F_{9/2} \rightarrow {}^4I_{15/2}$) with the populating (ETU3) [$^4I_{11/2} + {}^4I_{13/2} \rightarrow {}^4I_{15/2} + {}^4F_{9/2}$, CR1 ($^4F_{7/2} + {}^4I_{15/2} \rightarrow {}^4F_{9/2} + {}^4I_{13/2}$)] and depletion (ETU2) processes.

Figure 3(e) presents the decay luminescence from $^4G_{11/2}$ (379 nm), $^4F_{5/2}$ (449 nm), and $^4F_{7/2}$ (486 nm) levels for SrF_2:Er (1.6%). An almost immediate rise is observed in the time dependence of the UCL of Er^{3+} ions from these levels. These experimental results show that the dominant mechanisms in the populating of the $^4G_{11/2}$ and $^4F_{5/2}$ levels are the ESA1($^4S_{3/2} + h\nu \rightarrow {}^2G_{7/2}$) and ESA2($^4I_{9/2} + h\nu \rightarrow {}^4F_{3/2}$), respectively. Energy gaps between $^4G_{11/2}$ and $^4S_{3/2}$ levels as well as $^4F_{3/2}$ and $^4I_{9/2}$ levels correspond to the energy of the incident photon at a wavelength of 972 nm. The fast rise of the UCL from the $^4F_{7/2}$ level is explained by a strong influence of the cross-relaxation (CR1) and multi-phonon relaxation (MPR) on the depletion of this level. The near-infrared UCL from the $^4I_{9/2}$ (801 nm) level appears to correspond to the CR2 between the two levels $^4S_{3/2}$ and $^4I_{15/2}$ ($^4S_{3/2} + {}^4I_{15/2} \rightarrow {}^4I_{9/2} + {}^4I_{13/2}$).

To identify the mechanisms responsible for UCL of Er^{3+} ions in the SrF_2:Er upon excitation of the $^4I_{11/2}$ level, we also studied the excitation power density P-dependent UCL at the $^4S_{3/2} \rightarrow {}^4I_{15/2}$ (548 nm) and $^4F_{9/2} \rightarrow {}^4I_{15/2}$ (668 nm) transitions of the Er^{3+} ions (Fig. 4). It is well known[31] that the UCL intensity I_{UC} depends on the excitation power density P as $I_{UC} \propto P^n$, where n is the number of absorbed photons needed for populating the upper energy level of the transition. Pollnau *et al.*[31] investigated in detail the influence of the types of UC mechanisms on the slopes.

Figure 4 shows the log-log dependence of the UCL intensity on the LD excitation power density for the SrF_2:Er (1.6%) and SrF_2:Er (8.8%) samples. The slopes of the $^4S_{3/2} \rightarrow {}^4I_{15/2}$ [Fig. 4(a)] and $^4F_{9/2} \rightarrow {}^4I_{15/2}$ [Fig. 4(b)] transitions for SrF_2:Er (1.6%) are calculated to be 2.72 and

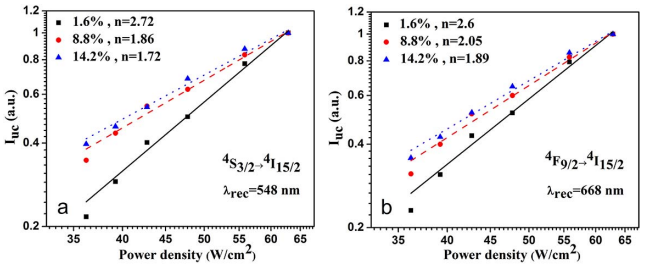

Fig. 4. P-dependent UCL at the (a) $^4S_{3/2} \rightarrow {}^4I_{15/2}$ and (b) $^4F_{9/2} \rightarrow {}^4I_{15/2}$ transitions of Er^{3+} ions. The diagram is in a double logarithmic scale.

2.6, respectively. These results indicate that the $^4S_{3/2} \rightarrow {}^4I_{15/2}$ and $^4F_{9/2} \rightarrow {}^4I_{15/2}$ transitions were mainly attributed to three-photon absorption processes at a low concentration of Er^{3+} ions (ETU1 or ETU2, ESA1 or ESA2). For SrF_2:Er (8.8%) the slopes of green and red luminescence are 1.86 and 2.05, respectively. This means that two-photon absorption processes [CP ($^4I_{11/2} + {}^4I_{11/2} + {}^4I_{15/2} \rightarrow {}^4I_{15/2} + {}^4I_{15/2} + {}^4F_{7/2}$)] are the dominant mechanisms of visible UCL for SrF_2:Er phosphors with high concentrations of Er^{3+} ions. As mentioned above, the rare-earth ions in MF_2:RE have a pronounced tendency to associate in clusters. At low rare-earth (Er^{3+}) concentrations (on the order of a few hundredths of a percent), oppositely charged point defects R^{3+} and F_{int} combine to form dipole pairs[32]. Increasing the rare-earth concentration in the solid solution leads to further defect association and defect clustering[13,33]. The concentration of clusters increases with increasing the RE concentration and the phenomenon of percolation begins from 6%[23]. As a result of this phenomenon, clusters come to inevitable spatial contact with each other. Thus, superclusters are formed, which reach a micron size. Rare-earth elements are concentrated in these superclusters. Apparently, SrF_2:Er phosphors at a high concentration are characterized by an increase in the clusters concentration. The presence of ion–ion interaction between Er^{3+} ions in neighboring clusters in these samples leads to an increase in probability of the cooperative process.

Next, the influence of the Er^{3+} concentration on the UCL intensity in the visible spectral range was studied. Figure 5(a) presents the spectral power of the UCL of Er^{3+} ions in the visible range upon laser excitation at

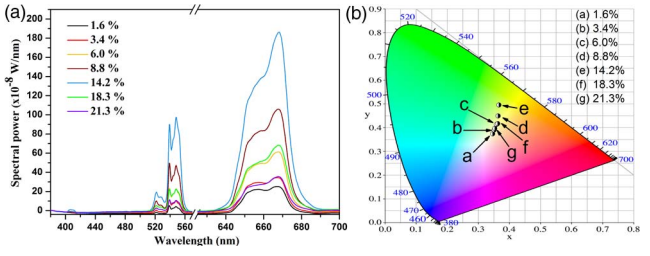

Fig. 5. (a) Spectral power of the UCL of SrF_2:Er. (b) The CIE chromaticity diagram of SrF_2:Er. The excitation power density is 63 W/cm^2.

972 nm for SrF_2:Er (mole fractions of Er^{3+} ions are 1.6%, 3.4%, 6.0%, 8.8%, 14.2%, 18.3%, and 21.3%).

It follows from Fig. 5(a) that the strongest UCL occurs when the concentration of Er^{3+} ions is 14.2 mol. %. Upon further increase of the concentration of Er^{3+} ions, the spectral power of the UCL begins to decrease. The ratio of red to green luminescence of Er^{3+} ions is the same for all SrF_2:Er samples.

SrF_2:Er phosphors could be used as infrared quantum counters, temperature sensors, visualizers of infrared laser radiation, phosphors for light-emitting diodes, and others. To develop UC phosphors for the above application fields, the luminescence efficiency, i.e., photoluminescence quantum yield needs to be investigated. The photoluminescence quantum yield is defined as the number of emitted photons per that of photons absorbed by luminescence materials. We have developed a system (see Section 2) for measuring UC photoluminescence quantum yield based on an absolute method[26,27].

The photoluminescence quantum yields of SrF_2:Er (mole fractions of Er^{3+} ions are 1.6%, 3.4%, 6.0%, 8.8%, 14.2%, 18.3%, and 21.3%) were measured upon excitation of a 972 nm LD with different power densities. The results of the measurement of Φ_{UC} are shown in Table 1.

The absolute quantum yield of SrF_2:Er phosphors increases with an increasing concentration of Er^{3+} ions up to 14.2%. The maximum quantum yield was achieved at 0.28% for SrF_2:Er (14.2 mol.%) with an incident laser power density of 63 W/cm^2.

The dependences of the quantum yield and intensity of the UCL on the concentration of Er^{3+} ions can be explained by UC mechanisms. Important quenching pathways of UCL of SrF_2:Er are radiative transitions $^4I_{9/2} \rightarrow {}^4I_{15/2}$, $^4I_{11/2} \rightarrow {}^4I_{13/2}$ and $^4I_{13/2} \rightarrow {}^4I_{15/2}$ of Er^{3+} ions. For example, efficient mid-infrared laser oscillations of SrF_2:Er crystals upon excitation of the $^4I_{11/2}$ level were demonstrated at room temperature[28,29]. The results of investigation of the excited-state dynamics and *P*-dependent UCL of the SrF_2:Er phosphors show that the probability of CP increases with increasing concentration of Er^{3+} ions. CP depopulates the $^4I_{11/2}$ level and populates the visible levels of the Er^{3+} ions. Thus, with an increasing concentration up to 14.2%, CP leads to a decrease in the mid-infrared quenching pathway of the UCL of SrF_2:Er and thereby increases the photoluminescence quantum yield. Reducing the quantum yield and intensity of the UCL of SrF_2:Er upon further increasing the concentration of Er^{3+} ions is explained by concentration quenching.

Increasing the power density leads to enhancing the UC quantum yield of SrF_2:Er because the probability of the UC processes also increases.

The chromaticity of the SrF_2:Er phosphors was calculated by use of the Commission International de l'Eclairage (CIE) chromaticity coordinates (x, y) and the results are presented in Fig. 5(b) and Table 1. The color temperatures for SrF_2:Er with 1.6%, 3.4%, 6.0%, 8.8%, 14.2%, 18.3%, and 21.3% concentrations of Er^{3+} ions were 4936, 4814, 4692, 4695, 4782, 4589, and 4783 K, respectively.

In summary, the mechanisms of UCL of SrF_2:Er phosphors corresponding to the $^4G_{11/2} \rightarrow {}^4I_{15/2}$, $^2H_{9/2} \rightarrow {}^4I_{15/2}$, $^4F_{5/2} \rightarrow {}^4I_{15/2}$, $^4F_{7/2} \rightarrow {}^4I_{15/2}$, $^2H_{11/2} \rightarrow {}^4I_{15/2}$, $^4S_{3/2} \rightarrow {}^4I_{15/2}$, $^4F_{9/2} \rightarrow {}^4I_{15/2}$ and $^4I_{9/2} \rightarrow {}^4I_{15/2}$ transitions upon excitation of the $^4I_{11/2}$ level of Er^{3+} ions were investigated for the first time. ETU processes are responsible for populating the $^2H_{9/2}$, $^2H_{11/2}$, $^4S_{3/2}$, and $^4F_{9/2}$ levels. CP is the dominant mechanism of UCL from the $^4S_{3/2}$ and $^4F_{9/2}$ levels for high concentrations of Er^{3+} ions. The UCL from $^4G_{11/2}$ and $^4F_{5/2}$ is explained by ESA. Cross-relaxation processes play a significant role in populating the $^4F_{9/2}$ and $^4I_{9/2}$ levels. For quantifying material performance the Er^{3+}-concentration dependence of UCL and absolute quantum yields of SrF_2:Er phosphors were studied. The most intensive visible luminescence was obtained for SrF_2:Er (14.2 mol.%) with a 0.28% maximum quantum yield. The present results indicate that SrF_2:Er prepared by using a co-precipitation from the aqueous nitrate solution is a promising UC phosphor.

Table 1. Quantum Yields, Chromaticity Coordinates x, y and Color Temperature T of SrF_2:Er Phosphors

Er^{3+} concentration (mol.%)	P (W/cm^2)	Φ_{UC} (%)	x	y	T (K)
1.6	25	–	0.3497	0.3548	4838
	63	–	0.3463	0.3470	4936
3.4	25	0.02	0.3498	0.3599	4858
	63	0.09	0.3515	0.3643	4814
6.0	25	0.10	0.3507	0.3722	4892
	63	0.16	0.3586	0.3888	4692
8.8	25	0.14	0.3527	0.4207	4961
	63	0.17	0.3639	0.4268	4695
14.2	25	0.17	0.3602	0.4795	4922
	63	0.28	0.3665	0.4753	4782
18.3	25	0.06	0.3546	0.4118	4887
	63	0.09	0.3627	0.3924	4589
21.3	25	0.03	0.3461	0.3765	5041
	63	0.04	0.3533	0.3712	4783

This work was supported by the Russian Science Foundation (No. 17-72-10163).

References

1. F. Vetrone and J. A. Capobianco, Int. J. Nanotechnol. **5**, 1306 (2008).
2. M. Misiak, M. Skowicki, T. Lipiński, A. Kowalczyk, K. Prorok, S. Arabasz, and A. Bednarkiewicz, Nano Res. **10**, 3333 (2017).

3. Z. Song, Y. G. Anissimov, J. Zhao, A. V. Nechaev, A. Nadort, D. Jin, T. W. Prow, M. S. Roberts, and A. V. Zvyagin, J. Biomed. Opt. **18**, 061215 (2013).
4. C. Portioli, M. Pedroni, D. Benati, M. Donini, R. Bonafede, R. Mariotti, L. Perbellini, M. Cerpelloni, S. Dusi, A. Speghini, and M. Bentivoglio, Nanomedicine **11**, 3039 (2016).
5. A. A. Lyapin, P. A. Ryabochkina, A. N. Chabushkin, S. N. Ushakov, and P. P. Fedorov, J. Lumin. **167**, 120 (2015).
6. A. A. Lyapin, P. A. Ryabochkina, S. N. Ushakov, and P. P. Fedorov, Quantum Electron. **44**, 602 (2014).
7. A. A. Lyapin, S. V. Kuznetsov, P. A. Ryabochkina, A. P. Merculov, M. V. Chernov, Y. A. Ermakova, A. A. Luginina, and P. P. Fedorov, Laser Phys. Lett. **14**, 076003 (2017).
8. C. M. Verber, D. R. Grieser, and W. H. Jones, J. Appl. Phys. **42**, 2767 (1971).
9. S. R. Bullock, B. R. Reddy, and P. Venkateswarlu, J. Opt. Soc. Am. B **14**, 553 (1997).
10. I. Richman, J. Chem. Phys. **41**, 2836 (1964).
11. D. J. M. Bevan, O. Greis, and J. Strahle, Acta Crystallogr. A **36**, 889 (1980).
12. P. P. Fedorov, Butll. Soc. Catalana Cienc. Fis. Quim. Mat. **12**, 349 (1991).
13. S. A. Kazanskii, A. I. Ryskin, A. E. Nikiforov, A. Y. Zaharov, M. Y. Ougrumov, and G. S. Shakurov, Phys. Rev. B **72**, 014127 (2005).
14. M. B. Seelbinder and J. C. Wright, Phys. Rev. B **20**, 4308 (1979).
15. N. Rakov, R. B. Guimarães, D. F. Franceschini, and G. S. Maciel, Mater. Chem. Phys. **135**, 317 (2012).
16. Y. Liu, D. Li, Q. Ma, X. Dong, X. Xi, W. Yu, X. Wang, J. Wang, and G. Liu, J. Mater. Sci. Mater. Electron. **27**, 5277 (2016).
17. F. Huang, L. Hu, and D. Chen, Ceram. Int. **41**, 189 (2015).
18. J. Zhang, S. Wang, T. Rong, and L. Chen, J. Am. Ceram. Soc. **87**, 1072 (2004).
19. C. Ma, J. Qiu, D. Zhou, Z. Yang, and Z. Song, Chin. Opt. Lett. **12**, 081601 (2014).
20. Y. Zhang, X. Wang, Y. Li, Y. Li, and X. Yao, Opt. Mater. Express **8**, 12 (2018).
21. O. Henderson-Sapir, J. Munch, and D. J. Ottaway, Opt. Express **24**, 6869 (2016).
22. Z. Chen, X. Zhang, S. Zeng, Z. Liu, Z. Ma, G. Dong, S. Zhou, X. Liu, and J. Qiu, Appl. Phys. Express **8**, 032301 (2015).
23. P. P. Fedorov, A. A. Luginina, S. V. Kuznetsov, and V. V. Osiko, J. Fluorine Chem. **132**, 1012 (2011).
24. P. P. Fedorov, S. V. Kuznetsov, M. N. Mayakova, V. V. Voronov, R. P. Ermakov, A. E. Baranchikov, and V. V. Osiko, Russ. J. Inorg. Chem. **56**, 1525 (2011).
25. M. N. Mayakova, A. A. Luginina, S. V. Kuznetsov, V. V. Voronov, R. P. Ermakov, A. E. Baranchikov, V. K. Ivanov, O. V. Karban, and P. P. Fedorov, Mendeleev Commun. **24**, 360 (2014).
26. A. Kobayashi, *Absolute Measurements of Photoluminescence Quantum Yields of Organic Compounds Using an Integrating Sphere* (Gunma University, 2010).
27. G. Gao, D. Busko, S. Kauffmann-Weiss, A. Turshatov, I. A. Howard, and B. S. Richards, J. Mater. Chem. **5**, 11010 (2017).
28. W. Ma, X. Qian, J. Wang, J. Liu, X. Fan, J. Liu, L. Su, and J. Xu, Sci. Rep. **6**, 36635 (2016).
29. J. Liu, J. Liu, Z. Guo, H. Zhang, W. Ma, J. Wang, and L. Su, Opt. Express. **24**, 30289 (2016).
30. F. Auzel, Chem. Rev. **104**, 139 (2004).
31. M. Pollnau, D. R. Gamelin, S. R. Lűthi, and H. U. Gűdel, Phys. Rev. B **61**, 3337 (2000).
32. C. G. Andeen, J. J. Fontanella, M. C. Wintersgill, P. J. Welcher, R. J. Kimble, and G. E. Matthews, J. Phys. C Solid State Phys. **14**, 3557 (1981).
33. M. Mujaji, G. D. Jones, and R. W. G. Syme, Phys. Rev. B **46**, 14398 (1992).